Transport properties and anomalous fatigue effect of $Ag/Bi_{0.9}La_{0.1}FeO_3$ /$La_{0.7}Sr_{0.3}MnO_3$ heterostructures*

Gao Rong-Li(高荣礼)[a)b)†], Fu Chun-Lin(符春林)[a)], Cai Wei(蔡 苇)[a)], Chen Gang(陈 刚)[a)]
Deng Xiao-Ling(邓小玲)[a)], Yang Huai-Wen(杨怀文)[b)], Sun Ji-Rong(孙继荣)[b)], and Shen Bao-Gen(沈保根)[b)]

[a)] *School of Metallurgy and Materials Engineering, Chongqing University of Science and Technology, Chongqing* 401331, *China*
[b)] *Beijing National Laboratory for Condensed Matter Physics, Institute of Physics, Chinese Academy of Sciences, Beijing* 100190, *China*

(Received 2 May 2014; revised manuscript received 14 May 2014; published online 23 July 2014)

The transport properties and fatigue effect of $Ag/Bi_{0.9}La_{0.1}FeO_3$ /$La_{0.7}Sr_{0.3}MnO_3$ heterostructures are described. By examining the *I*–*V* curves, an anomalous fatigue effect was found and its influences on resistive states were studied. *I*–*V* curves combined with *C*–*f* spectra were used to directly analyze the transport properties and fatigue effect. Compared to the first *I*–*V* cycle state, this structure shows more than one order increase of resistance after 100 cycles of "*I*–*V* curve training". The redistribution of oxygen vacancies in the depletion layer of $Ag/Bi_{0.9}La_{0.1}FeO_3$ is believed to be responsible for the different resistance mechanisms and tenfold magnitude drop in resistance. The resistive switching is understood to be caused by electric field–induced carrier trapping and detrapping, which changes the depletion layer thickness at the $Ag/Bi_{0.9}La_{0.1}FeO_3$ interface.

Keywords: transport properties, fatigue effect, switching, heterostructure

PACS: 77.22.Ej, 77.84.–s, 77.55.Nv, 77.90.+k **DOI:** 10.1088/1674-1056/23/9/097702

1. Introduction

In recent years, $BiFeO_3$ (BFO) has been extensively investigated due to its multiferroic properties and its potential applications in memory and magnetoelectric devices.[1,2] BFO is currently the most investigated multiferroic material that shows magnetoelectric coupling effects.[3,4] In particular, BFO is of considerable interest as a lead-free ferroelectric (FE) capacitor for commercial random access memories (FRAMs).[5,6] Resistive switching has been reported recently in BFO thin films,[7,8] the multiferroic properties of which have been intensively investigated.[9,10] However, a number of critical challenges remain and these need to be overcome before BFO-based thin films can be utilized for future memory devices. These challenges include lowering their leakage current, lowering their coercive field, and improving their reliability, particularly their resistance to fatigue. It is, therefore, interesting to study the resistive switching behavior and fatigue effect in BFO thin films in order to guide the design of multifunctional devices by combining ferroelectricity, ferromagnetism, and charge conduction. There have been many reports on the multiferroic properties and resistive switching behavior of BFO; however, only a few have focused on its fatigue, especially when "trained" by *I*–*V* cycles.

Moreover, from a technological point of view, one of the main problems which could limit the applications of this material is the high leakage current density. It has been reported that the existence of oxygen vacancies (V_{Os}), rather than Fe^{2+} ions, are the main cause of high leakage current in BFO films.[11–14] It has been proposed that the V_{Os} in BFO could be effectively reduced through the addition of chemical dopants and, in particular, La dopant. Doping at the Bi site could improve the crystallization and reduce the leakage of BFO.[15,16] Sandwiching BFO between two ferromagnetic metals may result in tunneling magnetoresistance and electroresistance, which could be controlled by both electric and magnetic fields, giving rise to a four-state memory device.[17,18] Therefore, BFO is a very important information storage material for fabricating future high-density magneto–electric random access memory. In the present work, the influence of the pulse voltage on the switching behavior of BFO thin films has been studied, and both the resistive switching and the rectifying behavior in BFO thin films were found to depend strongly on the voltage. However, until now there have been few studies of the training effect on the resistive switching and the change of resistance, especially in a case where the voltage is smaller than the coercive electric field in the *I*–*V* sweeping model. In this paper, we report the resistance switching and electrical properties, as well as an abnormal training effect. Bipolar resistive switching has been observed in a $Ag/Bi_{0.9}La_{0.1}FeO_3$ /$La_{0.7}Sr_{0.3}MnO_3$ sandwiched structure without any electroforming step. Based on the analysis of the transport characteristics during the switching, we discuss the switching mechanism, training characteristics, and the physical origin of volatility in the structures.

*Project supported by the Knowledge Innovation Project of the Chinese Academy of Sciences, the Beijing Municipal Natural Science Foundation, the National Natural Science Foundation of China (Grant Nos. 51102288 and 51372283), the Natural Science Foundation Project of Chongqing, China (Grant No. CSTC2012jjA50017), and the Cooperative Project of Academician Workstation of Chongqing University of Science & Technology, China (Grant Nos. CKYS2014Z01 and CKYS2014Y04).

†Corresponding author. E-mail: gaorongli2008@163.com

© 2014 Chinese Physical Society and IOP Publishing Ltd

2. Experimental process

Five hundred nanometer thick $Bi_{0.9}La_{0.1}FeO_3$ (BLFO) films were grown epitaxially on LSMO-coated (001) $SrTiO_3$ (STO) substrates using pulsed laser deposition (PLD). The target was prepared by mixing Bi_2O_3, La_2O_3, and Fe_2O_3 in a 1.1:0.1:1 stoichiometric ratio and sintering at 800 °C in air. An excess of Bi was used in order to compensate for the high volatility of Bi and prevent Bi deficiency. The conductive metallic oxide LSMO layer serves as the bottom electrode. First, a sintered stoichiometric LSMO target was employed for deposition of LSMO thin films on STO substrates under optimized growth conditions: a deposition temperature of 700 °C and an oxygen pressure about 50 Pa. It is pointed out that the LSMO film thickness is 30 nm. Then, the BLFO thin films were grown at 650 °C under a low oxygen pressure of 15 Pa. The laser output was about 1.5 J/cm^2, with a repetition rate of 5 Hz. Typical film growth rate was around 8 nm per minute. In order to ensure oxygen equilibrium, the films were slowly cooled to room temperature (2 °C /min) in an oxygen atmosphere of 100 Pa. Structural characterization of the BFO films was performed using X-ray diffraction (XRD), the surface roughness was analyzed by atomic force microscopy (AFM). In order to measure the electrical properties of the films, a 200-nm-thick Ag layer patterned with circles of 200-μm diameter was deposited on BLFO as the top electrodes by PLD through a shadow mask. The polarization–electric field (P–E) hysteresis loops were measured at room temperature using a ferroelectric test system (Radiant, Premier II). The current–voltage characteristics of Ag/BLFO/LSMO structures were measured at RT using a Keithley 2611 source meter system with voltage sweeping mode. The sweeping step is 0.1 V, and the sweeping speed is normal. During the measurement, a bias voltage was applied between the top (Ag) and bottom (LSMO) electrodes, with the latter being grounded. In this paper, applying a positive (negative) voltage on the top electrode is defined as a positive (negative) direction. The impedance (Z) and capacitance, were measured in the frequency range 40 Hz$< f < 10^8$ Hz using a precision impedance analyzer (Agilent 4294 A).

3. Results and discussion

Figure 1(a) shows the θ–2θ XRD patterns of the BLFO thin films grown on LSMO-coated STO (001) substrates. Only the (00l) (l = 1, 2, 3) peaks of BLFO, LSMO, and STO are visible, indicating a pure single-orientation perovskite BLFO phase. The out-of-plane c parameter for these films is c = 3.99 Å, which is very similar to the values obtained for undoped BFO films.[19,20] The surface was reasonably smooth with a root mean square (RMS) roughness of less than 0.6 nm, as shown in Fig. 1(b). Figure 2 shows P–E hysteresis loops measured at a frequency of 10 kHz, it can be seen that the maximal remanent polarization (Pr) reaches nearly 80 μC/cm^2 at the applied voltage of 36 V, which is slight bigger than the typical values of 60 μC/cm^2 obtained for BFO films.[21–24] It is noteworthy that the coercive field (E_c) increases with the applied electric field, and it is asymmetric in a positive and negative position. This asymmetric E_c has also been observed in BFO by other studies.[25] Although the origin of this anisotropy is not clear, it is likely to be due to a residual strain in the crystal or possibly to the difference in the inner fields on either side of the interface. In addition, the coercive field (about 300 kV/cm) is comparable to that of BFO thin films (Ref. [26]) but is almost one order of magnitude greater than that of BFO single crystals.[24] The large coercive field may originate from domain wall pinning and grain boundaries.

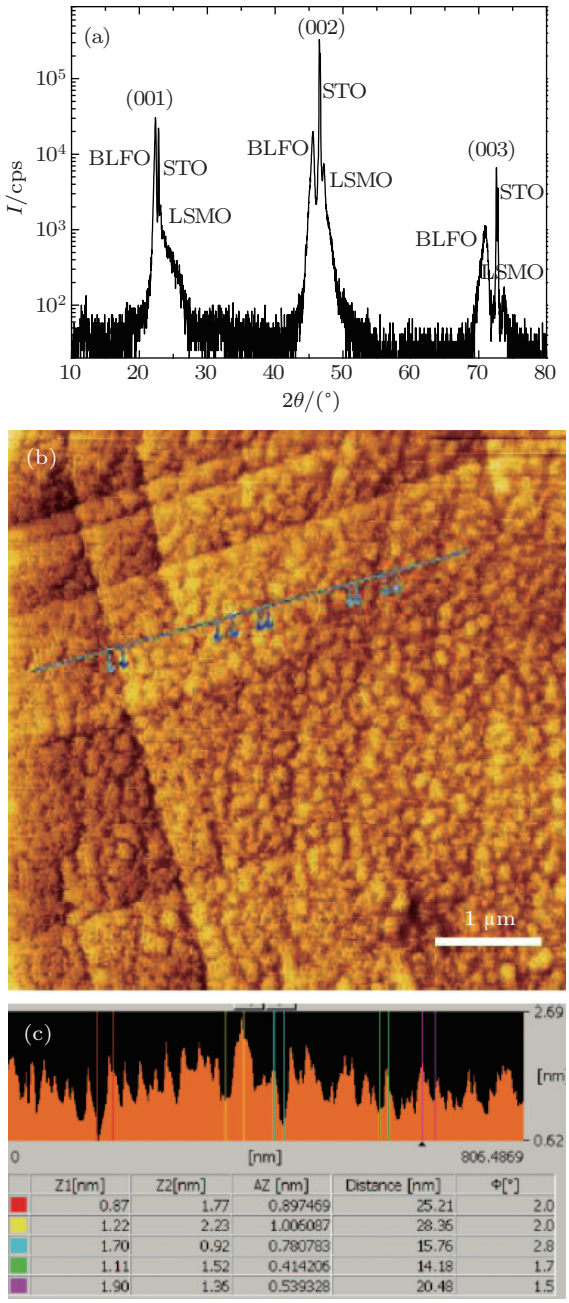


Fig. 1. (color online) (a) XRD spectrum of BLFO/LSMO/STO films with 2θ in the range of 10–80 degrees. (b) Topography images of the as-grown BLFO films. (c) The corresponding line roughness from panel (b).

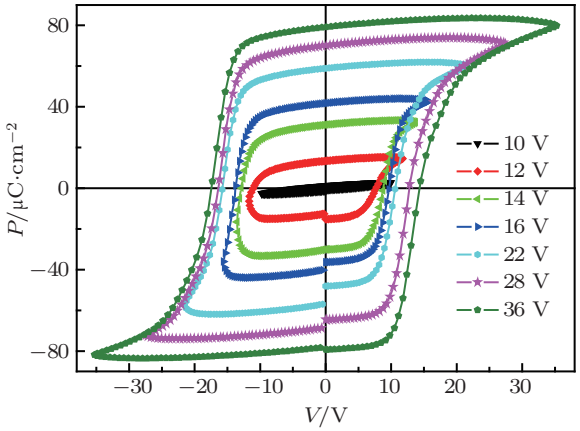


Fig. 2. (color online) Polarization versus voltage (P–V) curve of BLFO films at a frequency of 10 kHz at room temperature.

Owing to the high polarization in BLFO thin films, and its possible application in data storage, it is very important to understand the leakage current characteristics, especially the ratio of high and low resistance, as well as fatigue. Figure 3(a) shows the typical leakage current as a function of electrical field for the BLFO thin films by sweeping the voltage as 0 V→+6 V→ −6 V → 0 V. Prior to the I–V measurement, the sample was poled by +36 V and −36 V voltage pulse, respectively. As illustrated in Fig. 3(a), the I–V curves show rectifying characteristics with a rectification factor of 80 and 8 at ±6 V after polarized by −36 V and +36 V pulse voltage, respectively, indicating different polarized voltage attributions to different rectification factors. The pristine sample always exhibits a high resistance state (HRS) when a positive pulse voltage of +36 V is applied, while it can be switched to a low resistance state (LRS) by −36 V negative pulse voltage in the negative bias part.

To check the nonvolatility of the resistive switching observed in the I–V curves, pulsed voltage measurements were carried out. Writing pulses of ±36 V were applied to switch the resistance state of the stack between HRS and LRS, while the resistance state of the stack was detected using a small pulse voltage of −1.5 V and +1.5 V (reading pulse) (Figs. 3(b) and 3(c)), respectively. The resistance of both HRS and LRS was read repeatedly, more than 50 times, after either of them was written with 36 V and −36 V, respectively. In the as-switched case, both the LRS and the HRS read by ±1.5 V exhibit an increasing resistance. However, either state is stable after 10 repeated writes and reads; the corresponding LRS and the HRS read by +1.5 V is one-order of magnitude larger than that read by −1.5 V. In addition, it is observed that after 10 repeated writes and reads, the resistance ratio $R_{\rm HRS}/R_{\rm LRS}$ read by ±1.5 V decreased to 4. However, neither state exhibits significant resistance change if the write and read times are increased further. The retention measurement indicates that all of the resistance states are stable enough in time for memory applications. Note that, in the pulsed voltage measurement, although at −1.5 V a reading pulse has been repeatedly applied for resistance detection, the reading pulse is so much smaller than the coercive electric field of the BLFO film that it is unable to change the polarization state of the BLFO film, thus this relatively small voltage does not vary the resistance for either HRS and LRS. This is important for a practical memory application, which requires a stable resistance state, even if the unit is read many times.

In addition to the rectifying behavior, bipolar resistive switching is also observed in I–V cycles. No electroforming process is necessary before the observation of the hysteretic I–V curves. After the sweeping voltage reaches the maximum negative value (−6 V), it turns back to downward sweeping [e.g., process 4 in Fig. 3(a)] and the thin film has been set from HRS to the LRS. The thin film can be reset to HRS again by applying a positive sweeping bias voltage, as shown in Fig. 3(d). Note that, although the bipolar resistive switching can still be observed with the I–V sweeping cycles increased further, both the HRS and the LRS resistance increase and the resistance ratio $R_{\rm HRS}/R_{\rm LRS}$ read by −1.5 V decays exponentially by increasing the I–V cycle, that is, $R_{\rm HRS}/R_{\rm LRS}$ is only 4 after 100 I–V cycles, as shown in Fig. 3(e). This anomalous fatigue effect has not been reported before. On the other hand, the resistance state read by ±6 V increases with I–V cycles and has the same variation tendency: the resistance is close to saturation after 25 I–V cycles, as can be seen in Fig. 3(f).

To elucidate this switching mechanism and I–V fatigue, it is necessary to investigate the conduction mechanism for both the HRS and LRS. It is well known that, when positively charged oxygen vacancies (V_{Os}) attract electrons, the V_{Os} act as electron trapping centers.[27–30] Consider that, in both LRS and HRS, the barrier height of the BLFO/LSMO junction is always higher than that of the Ag/BLFO junction.[31] Thus, the current in the negative bias part is mainly limited by the Ag/BLFO interface. In LRS, after a negative sweeping bias is applied, more V_{Os} can be repelled to the Ag/BLFO interface. Therefore, more trapping centers are formed and occupied by electrons, favoring electron hopping. The electrons are easily injected into the depletion layer at the Ag/BLFO interface from the LSMO, significantly lowering the Ag/BLFO barrier. When the bias is reversed to positive, the electrons are blocked, such that much fewer electrons can be injected into the BLFO thin film from the LSMO bottom electrode. The poling with a positive bias can remove both V_{Os} and the trapped electrons from the Ag/BLFO interface, and is thus able to extend the depletion region in the pristine thin film, significantly increasing the resistance of the structure. Therefore, LRS and HRS can be observed in the following I–V measurement, as seen in Fig. 2(d), although the resistance state read by ±6 V increases with I–V cycles [Fig. 2(f)].

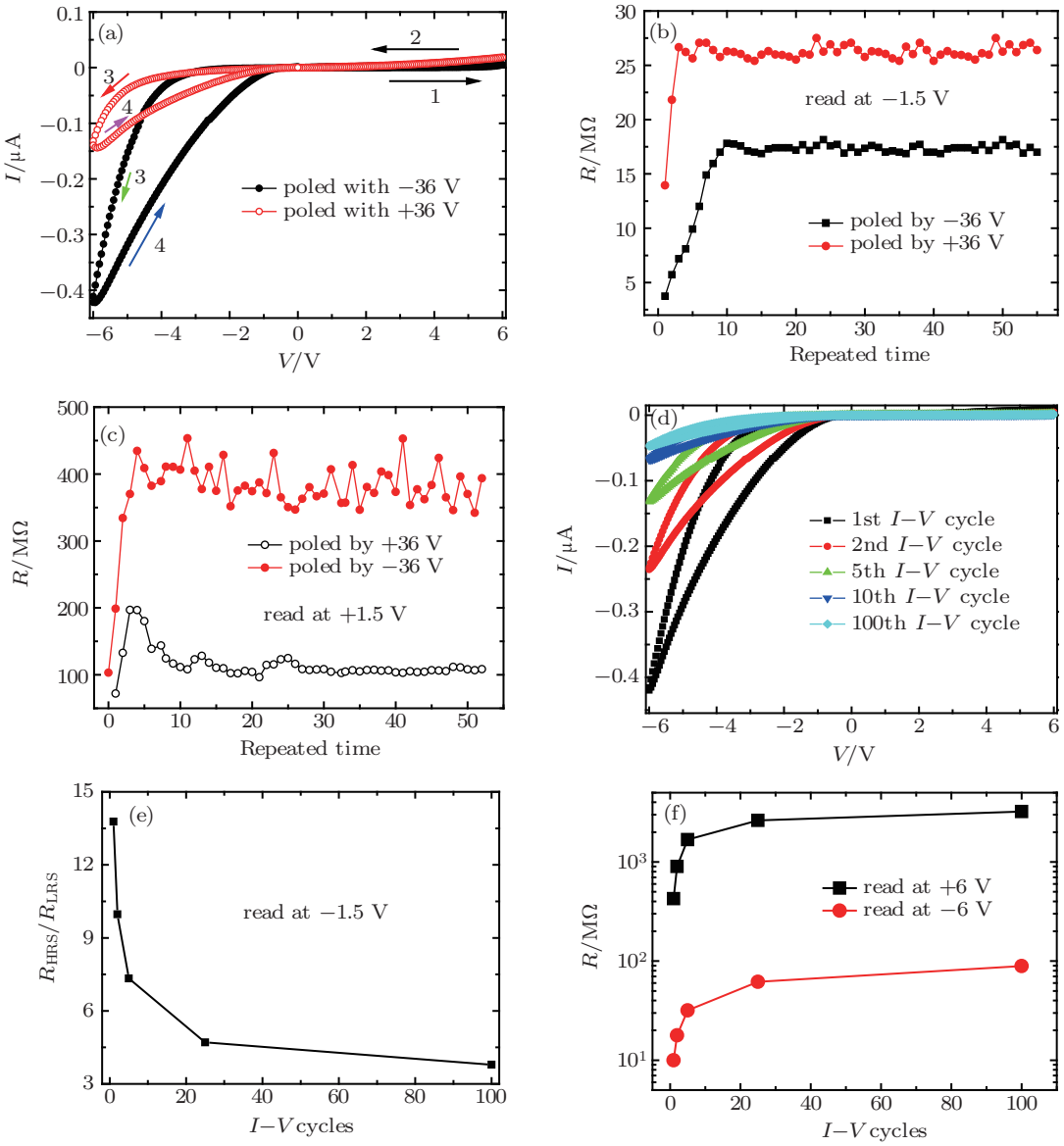


Fig. 3. (color online) (a) *I–V* curves after BLFO film polarized by +36 V and −36 V, respectively. (b) The resistance read by −1.5 V as a function of repeated written and read time. (c) Repeated written and read time dependence of the resistance read by +1.5 V. (d) *I–V* curves after different sweeping cycles. (e) The resistance ratio between HRS and LRS read at −1.5 V. (f) The resistance read by ±6 V as a function of *I–V* cycles.

To get further insight into the effect of the interface on the *I–V* fatigue curve, the change of the depletion width is demonstrated by the capacitance with an ac test level of 50 mV at 200 kHz. Figure 4(a) shows the capacitance as a function of repetitions after +36 V and −36 V poled, respectively, showing that the capacitance poled by −36 V (LRS) is bigger than that poled by +36 V (HRS). In the initial case, both the LRS and the HRS exhibit an decreasing capacitance. However, either state is stable after several repetitions. The capacitance in Fig. 4(a) and resistance in Figs. 3(b) and 3(c) with repetition have nearly the same trend, which indicates that the change of the resistance and capacitance is connected with the depletion width. In the case of *I–V* fatigue, the capacitance decreases with *I–V* cycles in the whole frequency range, while the decrease quantity drops with frequency, as shown in Figs. 4(b) and 4(c). The capacitance change is due to the modification of the depletion layer width, with obviously different *C–f* curves revealing different depletion thicknesses for LRS and HRS. The drop of the capacitance after positive voltage indicates the collapse of the depletion region. In the *C–f* measurement, the measured *C* is affected by many factors, such as measurement model (in parallel or in series) and the connected style of *C* and *R*. In addition, the resistance *R* arises from grain boundaries, grains, etc. Therefore, the capacitance in the *C–f* curves is contributed by the intrinsic capacitance and resistance.

In order to further verify the interaction between resistance and the depletion layer, the impedance spectra of the sample were further studied. The imaginary part of the frequency-dependent modulus (M''), calculated from the impedance Z^*, which is measured under −4 V, is shown in

Fig. 4(d). The peak maximum position is at $\omega = 1/RC$ with a peak height equal to $C_0/2C$, respectively.[31,32] Since the band bending of BLFO near the BLFO/LSMO interface will be flattened by the negative bias (−4 V), the impedance may be mainly contributed by the Ag/BLFO junction. It can be seen from Fig. 4(d) that the peak height decreased only a bit, whereas the peak position changes somewhat after 100 *I*–*V* cycles. This result implies that after the *I*–*V* cycle, the resistance increases obviously but capacitance increases only a little (the peak height decreases). Furthermore, it also means that the depletion of the Ag/BLFO interface has indeed been changed, which in turn affects the resistance. It should be pointed out that the capacitance increases but does not decrease in the M''–f spectrum, which is not consistent with the results from C–f curves, which happens because the capacitance in the C–f curves consists of not only the intrinsic capacitance but also the resistance.

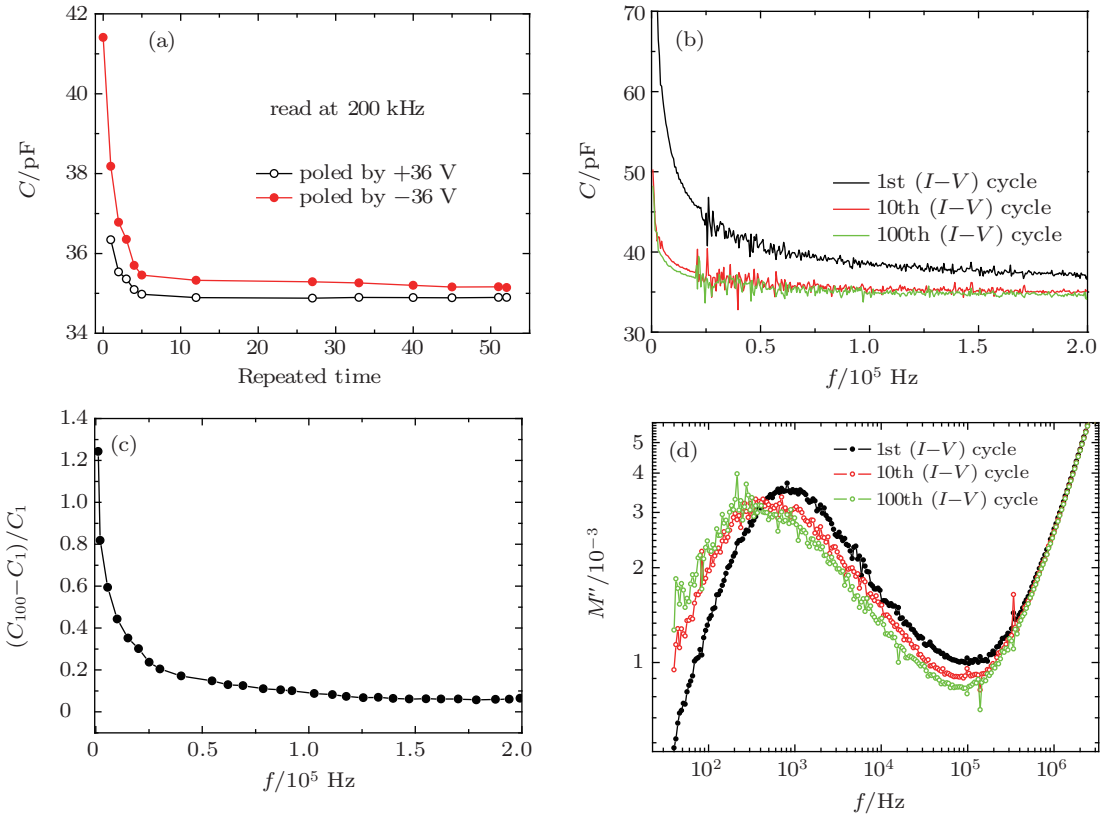


Fig. 4. (color online) (a) Capacitance as a function of repeated time after BLFO film polarized by +36 V and −36 V, respectively. (b) Frequency dependence of capacitance after different *I*–*V* cycles. (c) The capacitance variation as a function of frequency after 1 and 100 *I*–*V* cycles. (d) Frequency dependence of the electric modulus M'' (imaginary part) after 1, 10, and 100 *I*–*V* cycles.

The fatigue of the *I*–*V* cycle can be explained by means of a dynamic equilibrium process. After applying and removing the positive/negative bias, the depletion region extends to the Ag/BLFO interface and will increase/decrease back and forth. Consequently, the extension of the depletion layer will be in dynamic balance with the repulsion by generated electrons. This is a possible reason why the resistance needs several repetitions to stabilize, as can be observed in Fig. 3(b) to Fig. 3(e). Because the capacitance change is due to the modification of the depletion layer width, the fatigue of resistive switching is directly related to the dynamic balance of the depletion layer. It must be pointed out that the voltage used to measure the *I*–*V* curve is somewhat smaller than the coercive field, and is not large enough to switch the polarization. Therefore, the effect of ferroelectric polarization does not dominate the resistive switching in our BLFO thin films. The fatigue in the *I*–*V* cycle may not have the same origin as the polarization switching's fatigue characteristic.

4. Conclusions

In conclusion, the transport properties of $Bi_{0.9}La_{0.1}FeO_3$ thin film grown on $La_{0.7}Sr_{0.3}MnO_3$ have been described. According to *I*–*V* curves, an anomalous fatigue effect has been found and its influences on LRS and HRS states have been studied. *I*–*V* curves combined with *C*–*f* spectra were used to directly measure the transport properties. Compared to the first *I*–*V* cycle state, the structure's resistance increases more than one-order of magnitude after 100 cycles of "*I*–*V* curve training." It is believed that the redistribution of oxygen vacancies in the Ag/BLFO depletion layer is responsible for both

the different resistance mechanisms and for the drop in resistance. The resistive switching is understood by the electric field–induced carrier trapping and detrapping process, which changes the depletion layer thickness at the Ag/BLFO interface.

References

[1] Wang J, Neaton J B, Zheng H, Nagarajan V, Ogale S B, Liu B, Viehland D, Vaithyanathan V, Schlom D G, Waghmare U V, Spaldin N A, Rabe K M, Wuttig M and Ramesh R 2003 *Science* **299** 1719

[2] Zavaliche F, Zheng H, Mohaddes-Ardabili L, Yang S Y, Zhan Q, Shafer P, Reilly E, Chopdekar R, Jia Y, Wright P, Schlom D G, Suzuki Y and Ramesh R 2005 *Nano Lett.* **5** 1793

[3] Zhao T, Scholl A, Zavaliche F, Lee K, Barry M, Doran A, Cruz M P, Chu Y H, Ederer C, Spaldin N A, Das R R, Kim D M, Baek S H, Eom C B and Ramesh R 2006 *Nat. Mater.* **5** 823

[4] Lebeugle D, Colson D, Forget A, Viret M, Bataille A M and Gukasov A 2008 *Phys. Rev. Lett.* **100** 227602

[5] Scott J F 2007 *Science* **315** 954

[6] Singh S K, Ishiwara H and Maruyama K 2006 *Appl. Phys. Lett.* **88** 262908

[7] Yin K, Li M, Liu Y, He C, Zhuge F, Chen B, Lu W, Pan X and Li R W 2010 *Appl. Phys. Lett.* **97** 042101

[8] Yuan X Y, Luo L R, Wu D and Xu Q Y 2013 *Chin. Phys. B* **22** 107702

[9] Zhao T, Scholl A, Zavaliche F, Lee K, Barry M, Doran A, Cruz M P, Chu Y H, Ederer C, Spaldin N A, Das R R, Kim D M, Baek S H, Eom C B and Ramesh R 2006 *Nat. Mater.* **5** 823

[10] Catalan G and Scott J F 2009 *Adv. Mater.* **21** 2463

[11] Gao R L, Yang H W, Chen Y S, Sun J R, Zhao Y G and Shen B G 2014 *J. Alloy. Compd.* **591** 346

[12] Gao R L, Yang H W, Chen Y S, Sun J R, Zhao Y G and Shen B G 2014 *Appl. Phys. Lett.* **104** 031906

[13] Gao R L, Yang H W, Chen Y S, Sun J R, Zhao Y G and Shen B G 2014 *Europhys. Lett.* **105** 37008

[14] Pallkar V R, Kumara K G and Malik S K 2004 *Appl. Phys. Lett.* **84** 2856

[15] Ma Z Z, Li J Q, Tian Z M, Qiu Y and Yuan S L 2012 *Chin. Phys. B* **21** 107503

[16] Gong Y F, Wu P, Liu W F, Wang S Y, Liu G Y and Rao G H 2012 *Chin. Phys. Lett.* **29** 047701

[17] Béa H, Bibes M, Cherifi S, Nolting F, Warot-Fonrose B, Fusil S, Herranz G, Deralot C, Jacque E, Bouzehouane K and Barthélémy A 2006 *Appl. Phys. Lett.* **89** 242114

[18] Catalan G and Scott J F 2009 *Adv. Mater.* **21** 2463

[19] Béa H, Bibes M, Sirena M, Herranz G, Bouzehouane K, Jacquet E, Fusil S, Paruch P, Dawber M, Contour J P and Barthélémy A 2006 *Appl. Phys. Lett.* **88** 062502

[20] Dho J, Qi X D, Kim H, MacManus-Driscoll L J and Blamire M G 2006 *Adv. Mater.* **18** 1445

[21] Chu Y H, Zhan Q, Martin L W, Cruz M P, Yang P L, Pabst G W, Zavaliche F, Yang S Y, Zhang J X, Chen L Q, Schlom D G, Lin I N, Wu T B and Ramesh R 2006 *Adv. Mater.* **18** 2307

[22] Jang H W, Ortiz D, Baek S H, Folkman C M, Das R R, Shafer P, Chen Y, Nelson C T, Pan X Q, Ramesh R and Eom C B 2009 *Adv. Mater.* **21** 817

[23] Baek S H, Folkman C M, Park J W, Lee S, Bark C W, Tybell T and Eom C B 2011 *Adv. Mater.* **23** 1621

[24] Lebeugle D, Colson D, Forget A, Viret M, Bonville P, Marucco J F and Fusil S 2007 *Phys. Rev. B* **76** 024116

[25] Yi H T, Choi T, Choi S G, Oh Y S and Cheong S W 2011 *Adv. Mater.* **23** 3403

[26] Lahmar A, Habouti S, Dietze M, Solterbeck C H and Es-Souni M 2009 *Appl. Phys. Lett.* **94** 012903

[27] Shuai Y, Zhou S Q, Buŕger D, Helm M and Schmidt H 2011 *J. Appl. Phys.* **109** 124117

[28] Hu L, Sheng Z G, Huang Y N, Song W H and Sun Y P 2012 *Appl. Phys. Lett.* **101** 042413

[29] Huang X D, Feng Y J and Tang S 2012 *Acta Phys. Sin.* **61** 087702 (in Chinese)

[30] Sheng Z G, Sun Y P, Dai J M, Zhu X B and Song W H 2006 *Appl. Phys. Lett.* **89** 082503

[31] Gao R L, Chen Y S, Sun J R, Zhao Y G, Li J B and Shen B G 2012 *Appl. Phys. Lett.* **101** 152901

[32] Gao R L, Chen Y S, Sun J R, Zhao Y G, Li J B and Shen B G 2013 *J. Appl. Phys.* **113** 183510